

Auxetic piezoelectric effect in heterostructures

Received: 4 April 2023

Accepted: 23 October 2023

Published online: 30 November 2023

 Check for updatesMing-Min Yang^{1,2,3}✉, Tian-Yuan Zhu^{4,5}, Arne Benjamin Renz⁶,
He-Meng Sun^{2,3}, Shi Liu^{4,5}, Peter Michael Gammon⁶ & Marin Alexe¹✉

Inherent symmetry breaking at the interface has been fundamental to a myriad of physical effects and functionalities, such as efficient spin–charge interconversion, exotic magnetic structures and an emergent bulk photovoltaic effect. It has recently been demonstrated that interface asymmetry can induce sizable piezoelectric effects in heterostructures, even those consisting of centrosymmetric semiconductors, which provides flexibility to develop and optimize electromechanical coupling phenomena. Here, by targeted engineering of the interface symmetry, we achieve piezoelectric phenomena behaving as the electrical analogue of the negative Poisson’s ratio. This effect, termed the auxetic piezoelectric effect, exhibits the same sign for the longitudinal (d_{33}) and transverse (d_{31} , d_{32}) piezoelectric coefficients, enabling a simultaneous contraction or expansion in all directions under an external electrical stimulus. The signs of the transverse coefficients can be further tuned via in-plane symmetry anisotropy. The effects exist in a wide range of material systems and exhibit substantial coefficients, indicating potential implications for all-semiconductor actuator, sensor and filter applications.

The piezoelectric effect has been discovered and exploited in a wide range of materials with innate bulk non-centrosymmetric structures^{1–5}, such as ferroelectric oxides possessing morphotropic phase boundaries⁵, polymers⁶, two-dimensional layered materials⁷ and even bones⁸. Despite these materials’ diverse symmetries, structures, chemical natures and general material properties, the signs of their piezoelectric coefficients can hardly be modulated. The longitudinal (d_{33}) and the transverse (d_{31} , d_{32}) coefficients of the piezoelectric materials experimentally explored so far are of opposite signs (Supplementary Table 1). For example, the PbTiO_3 crystal has $d_{33} = 83.7 \text{ pC N}^{-1}$ and $d_{31} = -27.5 \text{ pC N}^{-1}$, whereas polyvinylidene difluoride films show $d_{33} \approx -20 \text{ pC N}^{-1}$ and $d_{31} \approx 20 \text{ pC N}^{-1}$ (refs. 9,10). These piezoelectric materials expand longitudinally along the electric field direction but contract transversally perpendicular to the field, or vice versa, exhibiting an electromechanical analogue of the positive Poisson’s ratio.

Piezoelectric materials with longitudinal and transverse coefficients sharing the same sign, that is, both being positive or negative, have not yet been experimentally demonstrated, to the best of our knowledge. It has been theoretically predicted that some materials, such as orthorhombic HfO_2 (belonging to the $Pca2_1$ symmetry group) and quasi-two-dimensional ternary compounds, ASnX ($A = \text{Na, K}$; $X = \text{N, P}$; $P6_3mc$) can possess both negative d_{33} and d_{31} , though experimental evidence remains absent¹¹. If realized, this exotic piezoelectric effect would be able to induce expansion or contraction in all directions under electric field stimulation. The effect would behave like the electrical analogue of auxetic materials showing a negative Poisson’s ratio^{12,13}.

In addition to the bulk asymmetry discussed above, inversion symmetry breaking at interfaces can also induce non-centrosymmetry-related physical effects, including the piezoelectric effect^{14–19}. Taking a Schottky junction as an example, the built-in field

¹Department of Physics, The University of Warwick, Coventry, UK. ²Hefei National Laboratory, Hefei, China. ³School of Emerging Technology, The University of Science and Technology of China, Hefei, China. ⁴Key Laboratory for Quantum Materials of Zhejiang Province, Department of Physics, School of Science and Research Center for Industries of the Future, Westlake University, Hangzhou, China. ⁵Institute of Natural Sciences, Westlake Institute for Advanced Study, Hangzhou, China. ⁶School of Engineering, The University of Warwick, Coventry, UK. ✉e-mail: mingminyang@hfnl.cn; M.Alexe@warwick.ac.uk

developed in the depletion region turns the semiconductor structure into a polar symmetry, regardless of the pristine symmetry of the semiconductor component. This gives rise to the interface piezoelectric effect, which arises from the synergy between the electrostriction effect and the electrical field, given as $d_{ijk} = 2M_{jkl}E_l$ (ref. 14) where i, j, k and l are direction index, described in more detail in the following. Concerning the case of the Schottky junction, its potential profile changes quadratically with distance from the metal–semiconductor interface, and the associated electric field decays linearly away from the interface. The effective electrical field is determined by the semiconductor properties, including the dielectric permittivity (χ) in the direction perpendicular to the interface (χ_3), the dopant density (N_d) and the built-in potential V_{bi} . Thus, the dependence of the piezoelectric coefficient d_{ijk} of a Schottky junction on its semiconductor properties can be expressed as follows¹⁴:

$$d_{ijk} = Q_{jki3}\chi_3\sqrt{2qN_d\chi_3V_{bi}} \quad (1)$$

where Q_{jki3} is the electrostriction coefficient ($M_{ijkl} = Q_{ijkl}\chi_k\chi_l$) and q is the elementary charge. The subscripts i, j, k and l are the elements of the right-handed coordinate direction group {1, 2, 3}. The direction 3 always refers to the direction normal to the Schottky junction interface, while 1 and 2 refer to the in-plane directions. Clearly, the controlling factors of the interface piezoelectric effect are distinctive from those of the bulk counterpart. Since χ_3 and $\sqrt{2qN_d\chi_3V_{bi}}$ are both positive, the sign of d_{ijk} is solely determined by the electrostriction coefficient Q_{jki3} (refs. 20–22). While the magnitude of the electrostriction coefficient can be optimized by chemical doping and the superlattice structure^{23,24}, it is predicted that the sign of electrostriction can be tuned by crystallographic orientation^{25,26}. We demonstrate that this crystallographic orientation dependence of the electrostriction effect can induce the auxetic piezoelectric effect at interfaces.

Phenomenological theory of the auxetic piezoelectric effect

To resolve this crystallographic orientation dependence, we take Nb:SrTiO₃ crystal as an example. Its electrostriction tensor Q_{ijkl}^0 in the (001) orientation has only three independent non-zero elements (that is, Q_{11}^0 , Q_{12}^0 and Q_{44}^0) with its coordinate axes x_0, y_0 and z_0 along the main crystallographic directions, that is, [100], [010] and [001]. When forming Schottky junctions on Nb:SrTiO₃ crystal with an orientation different from the most usual (001) orientation, the electrostriction tensor Q'_{ijkl} of the newly oriented device with a coordinate set xyz will be different from Q_{ijkl}^0 . The new coefficient Q'_{ijkl} can be derived from Q_{ijkl}^0 by tensor transformation using the correlation between their coordinate systems, which is given by

$$Q'_{ijkl} = R_{im}R_{jn}R_{kp}R_{lr}Q_{mnp}^0 \quad (2)$$

where R_{ij} is the transformation matrix elements between coordinate sets xyz and $x_0y_0z_0$. Details are given in the Methods and Supplementary Fig. 1. The subscripts m, n, p and r also refer to {1, 2, 3} and the Einstein summation is used here. The crystallographic-orientation-dependent piezoelectric coefficients d_{ijk} can be obtained by putting equation (2) into equation (1) and using the usual parameters of the Au/Nb:SrTiO₃ junctions prepared in our lab (for example, $\chi_3 = 1.68 \times 10^{-9} \text{ CV}^{-1} \text{ m}^{-1}$, $N_d = 2.4 \times 10^{25} \text{ m}^{-3}$ and $V_{bi} = 1.43 \text{ V}$). It is reasonable to assume that these parameters are independent of crystallographic orientation. As shown in the three-dimensional spherical polar plot (Fig. 1a), the longitudinal coefficient d_{33} of the Au/Nb:SrTiO₃ junction retains a positive value in all the crystallographic orientations, with its maxima at the <001> directions. On the other hand, both the sign and magnitude of the transverse coefficients d_{31} and d_{32} vary with orientation (Fig. 1b,c). Interestingly, they turn from classical negative values to positive at certain orientations, with their positive maxima appearing at some <110> directions.

To gain further insight, we extract a line profile of each piezoelectric coefficient, as indicated by the red line in Fig. 1a (line profiles are shown in Fig. 1d). Each profile corresponds to the crystal orientation (that is, the z axis) varying from (001) to (110) by sweeping angle θ between the z axis and z_0 axis from 0° to 90° (Fig. 1e). The formula expressing the dependence of d_{31} , d_{32} and d_{33} on the angle θ is given in the Methods.

As shown in Fig. 1d, d_{33} remains always positive with its maximum value at $\theta = 0^\circ$ (that is, the (001) orientation) and minimum at $\theta \approx 54.74^\circ$ (corresponding to the (111) orientation). The d_{31} value turns from negative to positive at about 45°, whereas d_{32} turns positive at about 27° and then returns to negative at $\approx 63^\circ$. The d_{31} and d_{32} values are equal to each other at the (001) and (111) orientations due to the in-plane isotropy at these two orientations. Based on the signs of the coefficients, especially those of d_{31} and d_{32} , one can classify the piezoelectric behaviour of the Au/Nb:SrTiO₃ junction into three different categories. In the first category, d_{33} is positive while both d_{31} and d_{32} are negative, corresponding to θ in the range of 0–27°, which is the same as in the conventional piezoelectric effect (Fig. 1f). The second category corresponds to θ in the range of 45–63°, wherein d_{31} , d_{32} and d_{33} are all positive. This means that an external field along the polar direction will induce expansion along all the directions, that is, the electrical analogue of a negative Poisson's ratio (Fig. 1g). This is the auxetic piezoelectric effect as proposed. The third category shows the in-plane anisotropy with one transverse coefficient being positive while the other one remains negative, corresponding to θ in the ranges of 27–45° or 63–90°. This type of piezoelectric effect gives rise to an expansion along the longitudinal direction and one in-plane direction but contraction along the other transverse direction when an external electrical field is applied (Fig. 1h). This exotic effect is referred to here as the 'type II' auxetic piezoelectric effect. The role of the electrostriction tensor in the manifestation of the auxetic piezoelectric effect, especially the key features of the tensor elements that ensure this emerging phenomenon, is further discussed in the Methods. In short, it is the anisotropy of the electrostriction coefficients, especially the ratio between Q_{11}^0 and Q_{44}^0 , that determines the manifestation of the auxetic piezoelectric effect. The larger the anisotropy, that is, the smaller Q_{44}^0/Q_{11}^0 , the more likely a show of the auxetic piezoelectric effect. Note that the auxetic piezoelectric effect demonstrated here is totally absent in conventional piezoelectric bulk materials, such as BaTiO₃, when one simply changes their device orientation, as is done here (Supplementary Fig. 2).

Experimental demonstration of the auxetic piezoelectric effect

Guided by the above phenomenological theory, we chose Au/Nb:SrTiO₃ Schottky junctions as the research object, with four crystallographic orientations: (001), (112), (111) and (110). These are representatives of the four angle ranges presented in Fig. 1d, which feature the piezoelectric effect with conventional, type II auxetic, auxetic and type II auxetic styles, respectively. These four interfaces with specific orientations possess a polar point symmetry of $4mm$, m , $3m$ and $mm2$, respectively. The fabrication details of these junctions are given in the Methods. To demonstrate the manifestation of the auxetic piezoelectric effect, especially the sign of the coefficients, we first used the direct piezoelectric effect, which detects the short-circuit current induced by the application of a uniform dynamic force or stress. (The demonstration of the converse auxetic piezoelectric effect will be discussed later.) We specifically used an aluminium electrode as an ohmic contact with Nb:SrTiO₃ crystals, playing the role of the counter electrode and forming a closed electrical circuit with the Schottky contact. The ohmic contact exhibits a negligible piezoelectric effect as demonstrated in our previous work¹⁴. To measure d_{33} , we applied a dynamic force on the Schottky junction surface via two gold-coated ultra-flat sapphire wafers and simultaneously read the output current. For the transverse coefficients (d_{31} , d_{32}), the dynamic force was applied to two parallel side planes, and we monitored the current output by the Schottky junctions.

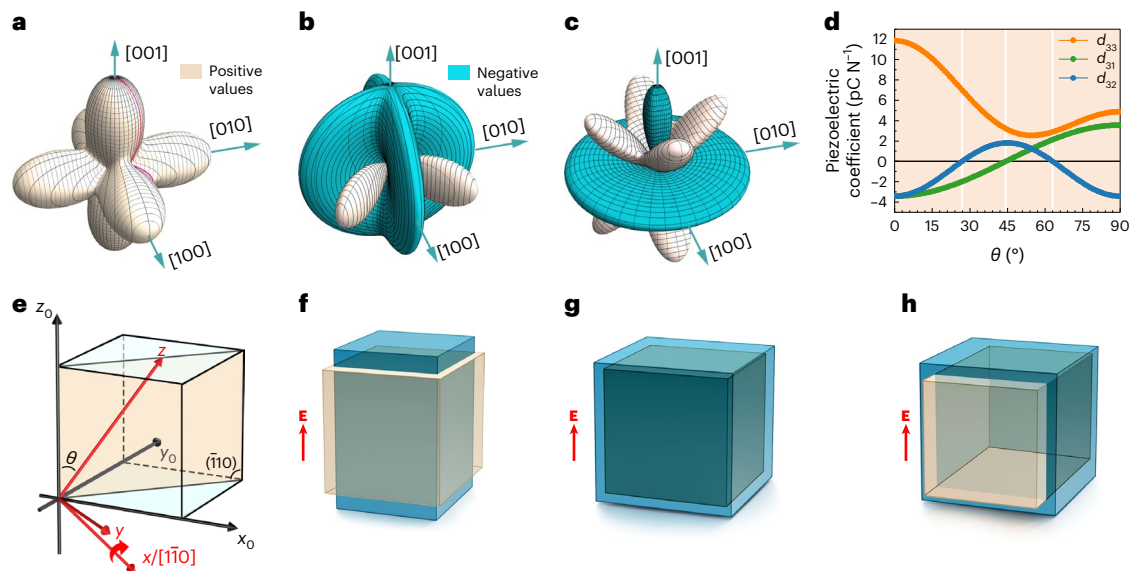


Fig. 1 Phenomenological theory of the auxetic piezoelectric effect.

a–c, Three-dimensional spherical polar plots of the crystallographic-orientation-dependent longitudinal piezoelectric coefficient d_{33} (**a**) and transverse coefficients d_{31} (**b**) and d_{32} (**c**) of Au/Nb:SrTiO₃ Schottky junctions. The tan colour indicates positive values while cyan indicates negative values. **d**, Angle (θ)-dependent piezoelectric coefficients d_{31} , d_{32} and d_{33} . **e**, Schematic showing the orientation varying from (001) to (110) within the ($\bar{1}10$) plane with angle θ

changing from 0° to 90°. Here, the x axis is along the $[\bar{1}10]$ crystallographic orientation. **f–h**, Schematics showing the lattice deformation under an external electrical field (E) in the conventional piezoelectric effect (**f**), auxetic piezoelectric effect (**g**) and type II auxetic piezoelectric effect (**h**). The tan and cyan cubes respectively refer to the structures before and after applying the external electric field.

Details of the set-up and measurement methods are given in the Methods and Supplementary Fig. 3. This approach, which characterizes the direct piezoelectric effect, is free from the entanglements of the electrostatic effect, electrochemical effect and strain-gradient effect, which usually occur in the characterization process of the converse piezoelectric effect^{27,28}.

We first compare the normal piezoelectric effect in a (001)-oriented Au/Nb:SrTiO₃ junction with that of a (111)-oriented junction. Figure 2a,b shows both the longitudinal and transverse piezo-response of the (001)-oriented Au/Nb:SrTiO₃ junction. For the sake of clarity, the amplitude of the dynamic stress applied to the samples is normalized to 1 MPa for both measurement geometries. The current induced in the longitudinal geometry (that is, d_{33}) exhibits a 90° phase shift with respect to the dynamic stress, while current related to the transverse geometry (that is, d_{31}) has a -90° phase shift, confirming the piezoelectric effect as the current generation mechanism and indicating the opposite signs between d_{33} and d_{31} . The exact value of d_{33} and d_{31} can be obtained by measuring the output current density as a function of the applied stress. The amplitude of the current density generated by both d_{33} and d_{31} increases linearly with the amplitude of the applied stress, confirming once more the piezoelectric nature. Based on the relation $J_3 = \omega d_{3i} \sigma_i$, where $\omega = 2\pi f$ and f is the frequency of applied stress, J_3 is the amplitude of the current density and σ_i is the stress amplitude, the value of the piezoelectric coefficients can be determined from the slope of J_3 versus σ_i . From the phase, which for both d_{33} and d_{31} remains constant over the measured stress range, we retrieve the sign of these coefficients. Thus, the values of d_{33} and d_{31} of the (001)-oriented Au/Nb:SrTiO₃ junction are 13.1 pC N^{-1} and -3.4 pC N^{-1} , respectively. The piezoelectric coefficients of this junction have been further confirmed by the frequency-dependent measurement, revealing a linear increase of the output current density with frequency at constant load (Supplementary Fig. 4). To compare these experimentally determined values with the theoretical values predicted by equations (1) and (2), the semiconductive properties of the junctions (that is, χ_3 , V_{bi} and N_d) were determined via current–voltage characteristics, capacitance–voltage characteristics and the Hall effect (Supplementary Fig. 5).

The theoretical piezoelectric coefficients yielded from equation (1) are $d_{33} = 12.2 \text{ pm V}^{-1}$ and $d_{31} = -3.5 \text{ pm V}^{-1}$, which are consistent with the experimental values. By contrast, the stress-induced current in the (111)-oriented Au/Nb:SrTiO₃ junction shows a 90° phase shift in both the longitudinal and transverse measurement geometries with respect to the dynamic stress, indicating the same sign between d_{33} and d_{31} (Fig. 2c). This phase shift is almost constant over a wide stress range (Fig. 2e) and frequency range (Supplementary Fig. 4). The respective experimental values of the piezoelectric coefficients are $d_{33} = 5 \text{ pC N}^{-1}$ and $d_{31} = 1.9 \text{ pC N}^{-1}$ (Fig. 2d), which are also close to the predicted values of $d_{33} = 6.0 \text{ pm V}^{-1}$ and $d_{31} = 2.9 \text{ pm V}^{-1}$ (Supplementary Fig. 5 and Supplementary Table 2). This is a direct experimental proof of the auxetic piezoelectric effect, that is, both positive longitudinal and positive transverse coefficients, in the (111)-oriented Nb:SrTiO₃ junction.

Demonstration of the type II auxetic piezoelectric effect

We applied dynamic stress to the parallel side planes of the (110)-oriented Au/Nb:SrTiO₃ junction along the $[\bar{1}10]$ and [001] crystallographic orientations, respectively, to characterize d_{31} and d_{32} (Fig. 3a,b). Figure 3c–e shows the transverse piezoelectric response under pulsed dynamic stress. When the pulsed stress is applied to the sample along the $[\bar{1}10]$ in-plane direction, the transient current output is negative; when the pulsed stress is withdrawn, the current output turns positive. However, when the stress is applied along the [001] direction, turning on the stress causes a positive peak current, while a negative peak current appears after turning off the stress. This result clearly confirms the opposite signs of the piezoelectric coefficients along the two orthogonal in-plane directions, that is, d_{31} and d_{32} . The values of the measured piezoelectric coefficients under sinusoidal stress are $d_{31} = 6.2 \text{ pC N}^{-1}$, $d_{32} = -6 \text{ pC N}^{-1}$ and $d_{33} = 9.3 \text{ pC N}^{-1}$, which are also consistent with the values predicted by phenomenological theory, confirming the type II auxetic piezoelectric effect (Supplementary Figs. 6 and 7 and Supplementary Table 3). In addition, the (112)-oriented Au/Nb:SrTiO₃ Schottky junction also shows the type II auxetic piezoelectric effect, as predicted. Details are given in Supplementary Fig. 8 and Supplementary Table 4.

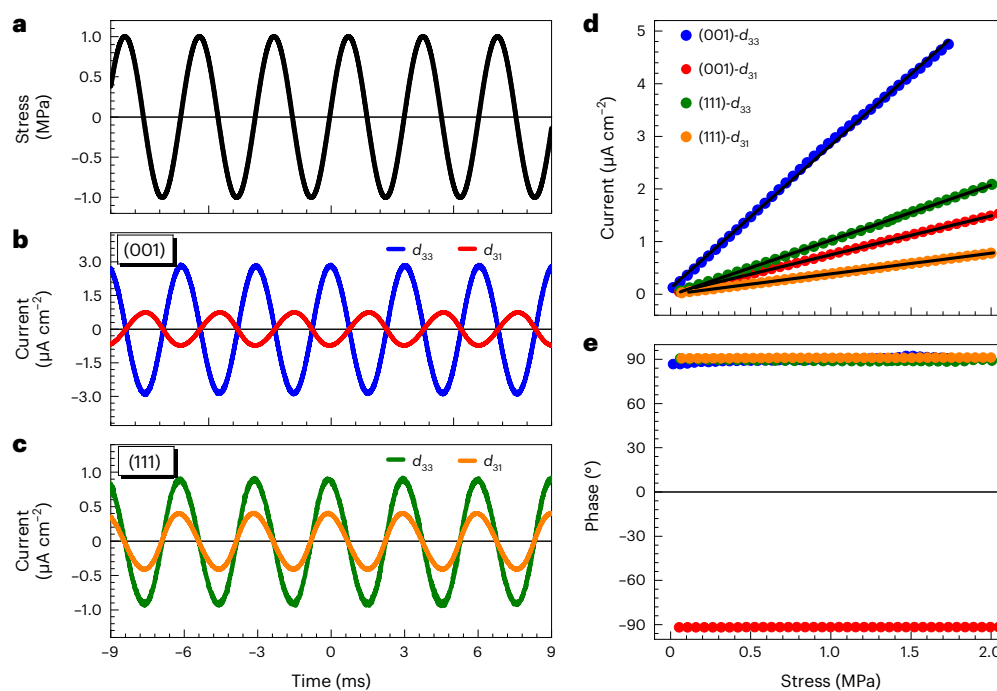


Fig. 2 | Experimental demonstration of the auxetic piezoelectric effect in Au/Nb:SrTiO₃ Schottky junctions. **a**, Measured waveform of applied sinusoidal stress. The positive and negative signs refer to tensile and compressive stress, respectively. **b**, Current density waveform output by a (001)-oriented Au/Nb:SrTiO₃ junction with the mechanical stress applied normal to the junction interface, that is, d_{33} (blue curve), and with the stress applied to the side planes

of the sample, that is, d_{31} (red curve). **c**, Current density waveform output by a (111)-oriented Au/Nb:SrTiO₃ junction in the d_{33} (green curve) and d_{31} (orange curve) measurement geometries, respectively. **d, e**, Load dependence of amplitude (**d**) and phase (**e**) of the current density output by the (001)- and (111)-oriented Au/Nb:SrTiO₃ junctions.

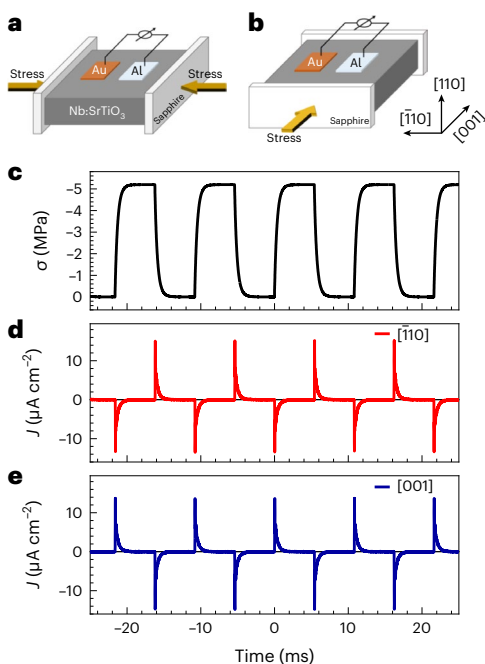


Fig. 3 | Demonstration of type II auxetic piezoelectric effect in (110)-oriented Au/Nb:SrTiO₃ Schottky junction. **a, b**, Schematics show the measurement geometries when force is applied along the $[1\bar{1}0]$ in-plane direction to measure d_{31} (**a**) and $[001]$ in-plane direction to measure d_{32} (**b**). **c**, Waveform of pulsed stress applied to side planes of the crystal. The stress amplitude (σ) has been normalized to 5 MPa. **d, e**, Piezoelectric current waveforms generated by the junction when stress is applied along the $[1\bar{1}0]$ in-plane direction (**d**; signal proportional to d_{31}) and $[001]$ in-plane direction (**e**; signal proportional to d_{32}).

Key features of the auxetic piezoelectric effect

Having demonstrated the two types of auxetic piezoelectric effect in Nb:SrTiO₃ Schottky junctions, we highlight four important features of the emergent phenomena. First, the auxetic piezoelectric effect demonstrated here also can be studied and elaborated on by density functional theory (DFT) calculations. Our DFT calculation replicates the auxetic behaviour of the (110)- and (111)-oriented SrTiO₃ heterostructures (Supplementary Figs. 9 and 10). More importantly, our calculation indicates that the auxetic piezoelectric effect at the oxide interfaces mainly originates from the domination of the internal-strain relaxation mechanism over the clamped-ion contribution (Supplementary Table 5).

Second, given the inherent inversion symmetry breaking at the interface, the auxetic piezoelectric effect is expected to occur in various heterostructures consisting of diverse components regardless of their pristine symmetry. In this regard, we have discovered similar piezoelectric behaviours in (001)- and (100)-oriented Nb:TiO₂ Schottky junctions. Rutile TiO₂ has a centrosymmetric $4/mmm$ tetragonal structure, with a symmetry-forbidden piezoelectric effect. Once a Schottky junction is formed on its (001)-oriented surface, the interface symmetry reduces to the polar tetragonal $4mm$ point group. On the other hand, forming a Schottky junction on the (100)-oriented surface turns the interface symmetry to the orthorhombic $mm2$ point group, showing a piezoelectric effect with in-plane anisotropy. The piezoelectric coefficients of the (001)-oriented Au/Nb:TiO₂ junction are measured to be $d_{31} = d_{32} = 2 \text{ pC N}^{-1}$ and $d_{33} = 5.9 \text{ pC N}^{-1}$, corresponding to the auxetic piezoelectric effect. The (100)-oriented Au/Nb:TiO₂ junction has piezoelectric coefficients of $d_{31} = 2.3 \text{ pC N}^{-1}$, $d_{32} = -1.5 \text{ pC N}^{-1}$ and $d_{33} = 3.4 \text{ pC N}^{-1}$, that is, the type II auxetic piezoelectric effect (Supplementary Figs. 11 and 12). In addition to the built-in field in the Schottky junctions, interface asymmetry can also be induced by

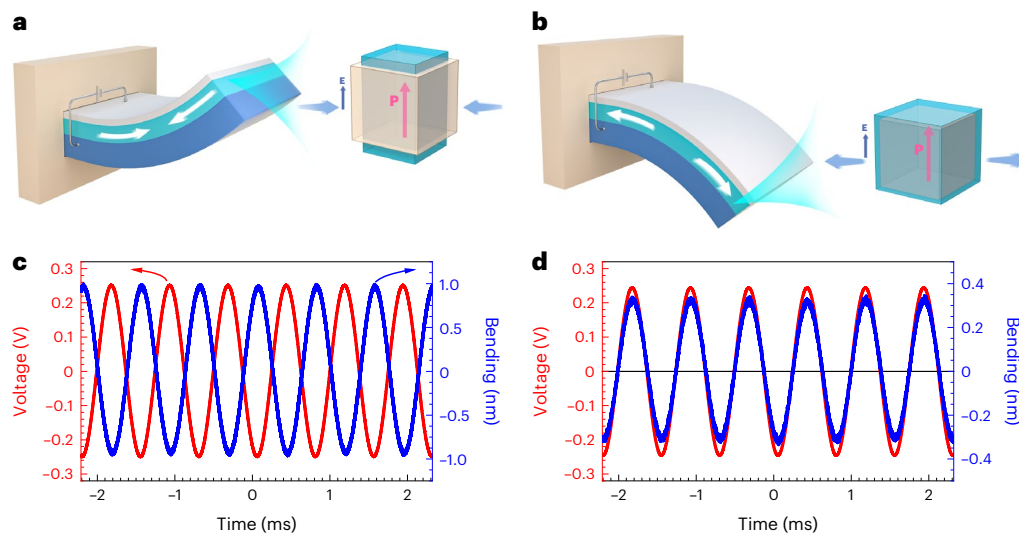


Fig. 4 | Demonstration of converse auxetic piezoelectric effect. **a**, Positive voltage induces upward bending in a cantilever with conventional piezo-active top layers. This cantilever is made of a piezo-inactive substrate, piezo-active layer and Pt top electrode. **b**, Auxetic piezoelectric effect induces downward bending. **P** refers to the induced electrical polarization arising from interface asymmetry.

c, Waveform of applied a.c. voltage and induced bending displacement at the end of the cantilever made of a (001)-SrTiO₃/Ba_{0.6}Sr_{0.4}TiO₃/BaTiO₃ superlattice grown on a Nb:SrTiO₃ substrate. **d**, The a.c.-voltage-induced vibration of a (111)-oriented superlattice cantilever. The frequency of the excitation signal here is 1.33 kHz, and the amplitude is 0.25 V.

many other stimuli, such as a strain gradient²⁹, compositional gradient³⁰, tricolour superlattices³¹ and so on. Among them, the tricolour superlattices possess an inherent inversion asymmetry and electrical polarization due to the particular (ABCABC...)-style stacking of their three different components, offering a fertile platform to explore and exploit effects and functionalities induced by interface asymmetry³¹. In this regard, we have prepared and studied (001)- and (111)-oriented SrTiO₃/Ba_{0.6}Sr_{0.4}TiO₃/BaTiO₃ superlattices with each layer of about 3 nm and a total thickness of about 100 nm. Details of the sample preparation and device characterization are given in the Methods. We discovered the auxetic piezoelectric effect in the (111)-oriented superlattice with effective piezoelectric coefficients of $d_{33} = 6.6 \text{ pC N}^{-1}$ and $d_{31} = 3.3 \text{ pC N}^{-1}$ (Supplementary Figs. 13–15). In comparison to Schottky junctions that have only one interface and limited functional thickness, the thickness of the tricolour superlattice can be designed as any rational value, which effectively turns the auxetic piezoelectric effect, which originates from interface asymmetry, to a bulk effect with no fundamental thickness limitation.

The auxetic piezoelectric effect demonstrated by the direct method also functions in the converse manner, converting electrical energy to mechanical energy. To demonstrate the converse auxetic piezoelectric effect, especially the transverse deformation under an external bias induced by d_{31} , we developed a voltage-induced bending measurement using a cantilever device configuration, which is similar to that of a piezoelectric bimorph actuator (Fig. 4a,b). Due to the opposite signs of the transverse piezo-coefficients d_{31} ($= d_{32}$), the conventional and auxetic piezo-effects will induce cantilevers that bend in opposite directions. Details of the measurement mechanism and technical details are given in the Methods. Figure 4c shows the vibration waveform of the (001)-oriented SrTiO₃/Ba_{0.6}Sr_{0.4}TiO₃/BaTiO₃ superlattice under the application of an a.c. voltage. The a.c. voltage and induced dynamic bending are $\sim 180^\circ$ out of phase. By contrast, the vibration of the (111)-oriented cantilever is fully in phase with the applied a.c. voltage (Fig. 4d). This difference relates to the opposite signs of the d_{31} values between the (001)- and (111)-oriented SrTiO₃/Ba_{0.6}Sr_{0.4}TiO₃/BaTiO₃ superlattices and proves the auxetic nature of the converse piezoelectric effect in the (111)-oriented tricolour superlattice. Further characterization and discussion of the cantilever vibration measurements are given in the Methods.

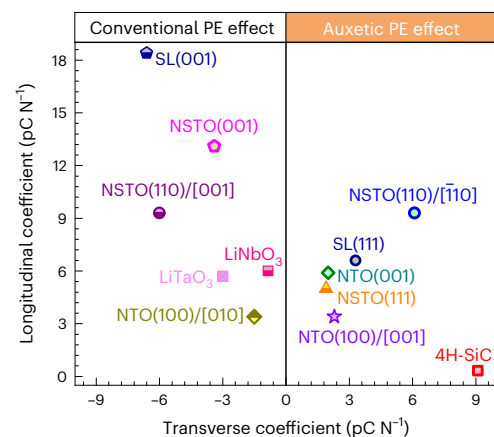


Fig. 5 | Summary of auxetic piezoelectric coefficients in heterostructures. Coefficients for conventional and auxetic piezoelectric (PE) effects are shown. NSTO refers to the Au/Nb:SrTiO₃ Schottky junction; NTO refers to the Au/Nb:TiO₂ Schottky junction; SL refers to the SrTiO₃/Ba_{0.6}Sr_{0.4}TiO₃/BaTiO₃ tricolour superlattice; 4H-SiC refers to the Mo/4H-SiC junction. The index enclosed by parentheses refers to the device orientation, while the index enclosed in brackets refers to the transverse direction along which force is applied. Data of LiNbO₃ and LiTaO₃ crystals are from ref. 32.

The auxetic piezoelectric effect is of technical importance. For example, the exotic piezoelectric effect demonstrated here can be potentially applied in acoustic wave devices. The great flexibility in tuning its piezoelectric coefficients would facilitate the elimination of spurious modes of acoustic wave filters. As demonstrated in Fig. 1b,c and Supplementary Fig. 16, we can tune the transverse piezoelectric coefficients to zero in the (110)-Au/Nb:SrTiO₃ junction if we set the in-plane edge directions along $[\bar{1}\bar{1}\sqrt{2}]$ and $[\bar{1}\bar{1}\sqrt{2}]$. In this specified crystallographic geometry design, an external field applied to the heterostructure will not induce transverse deformation, leaving this direction electromechanically inactive. In addition, being universal in nature, the auxetic piezoelectric effect allows us to explore and exploit this effect in materials compatible to complementary metal-oxide semiconductor technology. In this regard, we have explored

heterostructures based on (0001)-oriented 4H-SiC. Despite being innately a polar material with 6mm point symmetry, the high carrier density and conductivity of the as-grown 4H-SiC prohibit its application in electromechanical devices. However, by forming a Schottky junction with Mo electrodes, we discovered the auxetic piezoelectric behaviour, with $d_{31} = 9.1 \text{ pC N}^{-1}$ and $d_{33} = 0.32 \text{ pC N}^{-1}$ (Fig. 5 and Supplementary Fig. 17). The fabrication details and generic characterization are given in the Methods. Interestingly, while the d_{33} value is rather small, the d_{31} value is very large. It is three times larger than that of LiTaO₃ crystal and one order of magnitude larger than that of LiNbO₃, the latter two being the workhorses in filters of communication devices³². Together with the wafer-fabrication-compatible nature and extraordinary mechanical properties, this auxetic piezoelectric effect of the Mo/SiC junction possesses great potential in applications such as all-semiconductor surface acoustic wave filters, sensors, actuators and so on³³.

In summary, the pronounced tunability of the heterostructure interfaces facilitates the precise control of their electromechanical behaviors, leading to the discovery of the auxetic piezoelectric effect—a phenomenon that acts as the electrical counterpart to the negative Poisson's ratio. These results will allow us to explore the piezoelectric effect in a wide range of established semiconductor materials and heterostructure configurations. Thus, the results offers innovative approaches to design and optimize electromechanical devices compatible with complementary metal–oxide semiconductor technology.

Online content

Any methods, additional references, Nature Portfolio reporting summaries, source data, extended data, supplementary information, acknowledgements, peer review information; details of author contributions and competing interests; and statements of data and code availability are available at <https://doi.org/10.1038/s41563-023-01736-5>.

References

- Curie, J. & Curie, P. Développement par compression de l'électricité polaire dans les cristaux hémihédres à faces inclinées. *Bull. Minéral.* **3**, 90–93 (1880).
- Vanderbilt, D. Berry-phase theory of proper piezoelectric response. *J. Phys. Chem. Solids* **61**, 147–151 (2000).
- Saghi-Szabo, G., Cohen, R. E. & Krakauer, H. First-principles study of piezoelectricity in PbTiO₃. *Phys. Rev. Lett.* **80**, 4321–4324 (1998).
- Pan, H. et al. Ultrahigh-energy density lead-free dielectric films via polymorphic nanodomain design. *Science* **365**, 578–582 (2019).
- Li, F. et al. Giant piezoelectricity of Sm-doped Pb(Mg_{1/3}Nb_{2/3})O₃-PbTiO₃ single crystals. *Science* **364**, 264–268 (2019).
- Katsouras, I. et al. The negative piezoelectric effect of the ferroelectric polymer poly(vinylidene fluoride). *Nat. Mater.* **15**, 78–84 (2016).
- You, L. et al. Origin of giant negative piezoelectricity in a layered van der Waals ferroelectric. *Sci. Adv.* **5**, eaav3780 (2019).
- Fukada, E. & Yasuda, I. On the piezoelectric effect of bone. *J. Phys. Soc. Jpn* **12**, 1158–1162 (1957).
- Li, Z., Grimsditch, M., Xu, X. & Chan, S.-K. The elastic, piezoelectric and dielectric constants of tetragonal PbTiO₃ single crystals. *Ferroelectrics* **141**, 313–325 (1993).
- Jean-Mistral, C., Basrour, S. & Chailout, J. Comparison of electroactive polymers for energy scavenging applications. *Smart Mater. Struct.* **19**, 085012 (2010).
- Liu, J., Liu, S., Yang, J.-Y. & Liu, L. Electric auxetic effect in piezoelectrics. *Phys. Rev. Lett.* **125**, 197601 (2020).
- Lakes, R. Foam structures with a negative Poisson's ratio. *Science* **235**, 1038–1040 (1987).
- Evans, K. E. & Alderson, A. Auxetic materials: functional materials and structures from lateral thinking! *Adv. Mater.* **12**, 617–628 (2000).
- Yang, M.-M., Luo, Z.-D., Mi, Z., Zhao, J. & Alexe, M. Piezoelectric and pyroelectric effects induced by interface polar symmetry. *Nature* **584**, 377–381 (2020).
- Hwang, H. Y. et al. Emergent phenomena at oxide interfaces. *Nat. Mater.* **11**, 103–113 (2012).
- Soumyanarayanan, A., Reyren, N., Fert, A. & Panagopoulos, C. Emergent phenomena induced by spin–orbit coupling at surfaces and interfaces. *Nature* **539**, 509–517 (2016).
- Hellman, F. et al. Interface-induced phenomena in magnetism. *Rev. Mod. Phys.* **89**, 025006 (2017).
- Akamatsu, T. et al. A van der Waals interface that creates in-plane polarization and a spontaneous photovoltaic effect. *Science* **372**, 68–72 (2021).
- Ma, C. et al. Intelligent infrared sensing enabled by tunable moiré quantum geometry. *Nature* **604**, 266–272 (2022).
- Devonshire, A. Theory of ferroelectrics. *Adv. Phys.* **3**, 85–130 (1954).
- Uchino, K., Nomura, S., Cross, L. E., Jang, S. & Newnham, R. Electrostrictive effect in lead magnesium niobate single crystals. *J. Appl. Phys.* **51**, 1142–1145 (1980).
- Li, F., Jin, L., Xu, Z. & Zhang, S. Electrostrictive effect in ferroelectrics: an alternative approach to improve piezoelectricity. *Appl. Phys. Rev.* **1**, 011103 (2014).
- Zhang, H. et al. Atomically engineered interfaces yield extraordinary electrostriction. *Nature* **609**, 695–700 (2022).
- Korobko, R. et al. Giant electrostriction in Gd-doped ceria. *Adv. Mater.* **24**, 5857–5861 (2012).
- Kvasov, A. & Tagantsev, A. K. Positive effective Q₁₂ electrostrictive coefficient in perovskites. *J. Appl. Phys.* **112**, 094106 (2012).
- Nye, J. F. *Physical Properties of Crystals: Their Representation by Tensors and Matrices* (Oxford Univ. Press, 1985).
- Seol, D., Kim, B. & Kim, Y. Non-piezoelectric effects in piezoresponse force microscopy. *Curr. Appl. Phys.* **17**, 661–674 (2017).
- Abdollahi, A., Domingo, N., Arias, I. & Catalan, G. Converse flexoelectricity yields large piezoresponse force microscopy signals in non-piezoelectric materials. *Nat. Commun.* **10**, 1266 (2019).
- Lee, D. et al. Giant flexoelectric effect in ferroelectric epitaxial thin films. *Phys. Rev. Lett.* **107**, 057602 (2011).
- Damodaran, A. R. et al. Large polarization gradients and temperature-stable responses in compositionally-graded ferroelectrics. *Nat. Commun.* **8**, 14961 (2017).
- Sai, N., Meyer, B. & Vanderbilt, D. Compositional inversion symmetry breaking in ferroelectric perovskites. *Phys. Rev. Lett.* **84**, 5636–5639 (2000).
- Smith, R. & Welsh, F. Temperature dependence of the elastic, piezoelectric, and dielectric constants of lithium tantalate and lithium niobate. *J. Appl. Phys.* **42**, 2219–2230 (1971).
- Matthews, H. *Surface Wave Filters: Design, Construction, and Use* (John Wiley & Sons, 1977).

Publisher's note Springer Nature remains neutral with regard to jurisdictional claims in published maps and institutional affiliations.

Open Access This article is licensed under a Creative Commons Attribution 4.0 International License, which permits use, sharing, adaptation, distribution and reproduction in any medium or format, as long as you give appropriate credit to the original author(s) and the source, provide a link to the Creative Commons license, and indicate if changes were made. The images or other third party material in this article are included in the article's Creative Commons license, unless indicated otherwise in a credit line to the material. If material is not included in the article's Creative Commons license and your intended use is not permitted by statutory regulation or exceeds the permitted use, you will need to obtain permission directly from the copyright holder. To view a copy of this license, visit <http://creativecommons.org/licenses/by/4.0/>.

© The Author(s) 2023

Methods

Phenomenological theory of auxetic piezoelectric effect

The transformation matrix \mathbf{R} between the default coordinate set $\{x_0, y_0, z_0\}$ and the new set $\{x, y, z\}$ used in Fig. 1 of the main text is given as follows:

$$\mathbf{R} = \begin{bmatrix} \frac{\cos \beta + \sin \beta}{\sqrt{2}} & \frac{-\cos \beta + \sin \beta}{\sqrt{2}} & 0 \\ \frac{\cos \theta (\cos \beta - \sin \beta)}{\sqrt{2}} & \frac{\cos \theta (\cos \beta + \sin \beta)}{\sqrt{2}} & -\sin \theta \\ \frac{(\cos \beta - \sin \beta) \sin \theta}{\sqrt{2}} & \frac{(\cos \beta + \sin \beta) \sin \theta}{\sqrt{2}} & \cos \theta \end{bmatrix} \quad (3)$$

where θ is the angle between the z axis and z_0 axis, and β is the angle between x and the $[1\bar{1}0]$ crystallographic direction (Supplementary Fig. 1). With this setting, the x axis always remains in the x_0y_0 plane. Figure 1d in the main text corresponds to the scenario when $\beta = 0$ and the right-handed coordinate axis are rotated along the $[1\bar{1}0]$ axis.

Based on equations (1)–(3), the dependence of the Au/Nb:SrTiO₃ Schottky junction piezoelectric coefficients d_{333} , d_{311} and d_{322} on angle θ can be resolved as follows:

$$d_{333} = \frac{1}{2} [2Q_{11}^0 \cos^4 \theta + (Q_{11}^0 + Q_{12}^0 + 2Q_{44}^0) \sin^4 \theta + (Q_{12}^0 + 2Q_{44}^0) \sin^2 2\theta] \chi_3 \sqrt{2qN_d \chi_3 V_{bi}} \quad (4)$$

$$d_{311} = [Q_{12}^0 \cos^2 \theta + \frac{1}{2} (Q_{11}^0 + Q_{12}^0 - 2Q_{44}^0) \sin^2 \theta] \chi_3 \sqrt{2qN_d \chi_3 V_{bi}} \quad (5)$$

$$d_{322} = \frac{1}{16} [3Q_{11}^0 + 13Q_{12}^0 - 6Q_{44}^0 + (-3Q_{11}^0 + 3Q_{12}^0 + 6Q_{44}^0) \cos 4\theta] \chi_3 \sqrt{2qN_d \chi_3 V_{bi}} \quad (6)$$

In addition to the centrosymmetric cubic semiconductor represented by Nb:SrTiO₃, the phenomenological theory represented by equations (1) and (2) in the main text is applicable to semiconductors of any symmetry. In other words, the methodology developed here for Nb:SrTiO₃ junctions as a generic example can be readily transferred to the case of other semiconductor Schottky junctions, such as the Nb:TiO₂ junction, with minor modifications related to the dielectric permittivity. In the case of Nb:SrTiO₃, its dielectric permittivity is independent of the crystallographic orientation and can be treated as a constant since its permittivity tensor has only one independent non-zero element. However, rutile TiO₂ crystal has two independent non-zero elements in its permittivity tensor, that is, χ_{11} and χ_{33} . Thus, the dielectric constant of TiO₂ is dependent on the crystallographic orientation and cannot be treated as a simple scalar. One needs to calculate the orientation dependence of the dielectric permittivity via tensor transformation, as well, which is given by

$$\chi'_{ij} = R_{im} R_{jn} \chi_{mn} \quad (7)$$

where R_{im} is the transformation matrix given in equation (3).

Note that the auxetic piezoelectric effect of a Schottky junction induces the same volume change as that of the conventional piezoelectric effect when an external voltage is applied. To elucidate the volume effect, we use Schottky junctions composed of a cubic semiconductor as the example, such as the Nb:SrTiO₃ crystal. The dimension of the junctions stays constant as length \times width \times thickness = $a \times a \times t$. The volume variation when a unit external bias is applied to the junction along the thickness direction can be given as follows:

$$\Delta V = a^2 \left(1 + \frac{1}{t} d_{31}\right) \left(1 + \frac{1}{t} d_{32}\right) (t + d_{33}) - a^2 t. \quad (8)$$

Since junction length/width and thickness are respectively on the scale of 100 μm and 100 nm, $1 \gg \frac{1}{t} d_{31}$ and $1 \gg \frac{1}{t} d_{32}$. Thus, the above equation can be simplified to

$$\Delta V = a^2 (d_{31} + d_{32} + d_{33}). \quad (9)$$

Note that, although the respective value of d_{31} , d_{32} and d_{33} of the Schottky junctions changes while varying the crystallographic orientation as shown in Fig. 1 of the main text, the sum of d_{31} , d_{32} and d_{33} retains a constant value, given as follows:

$$d_{31} + d_{32} + d_{33} = (Q_{11}^0 + 2Q_{12}^0) \chi_3 \sqrt{2qN_d \chi_3 V_{bi}}. \quad (10)$$

This indicates that the auxetic piezoelectric effect induces the same volume change as the conventional piezoelectric effect in Schottky junctions consisting of the same type of cubic semiconductors. Therefore, the auxetic piezoelectric effect requires the same elastic energy cost compared to the conventional piezoelectric response in terms of volume change.

The role of electrostriction coefficients on the auxetic piezoelectric effect

Variation of the electrostriction coefficients with respect to the crystallographic orientation plays an essential role in the manifestation of the auxetic piezoelectric effect. Thus, it is important to elucidate the way to specify or design materials with certain electrostriction tensors that can show the auxetic piezoelectric effect at their interfaces. To this end, we would like to first discuss the case of Schottky junctions composed of centrosymmetric cubic semiconductors, such as Nb:SrTiO₃ and silicon. The methodology used for this type of material can then be generalized to other crystallographic structures, with some minor modifications.

The crystallographic-orientation-dependent piezoelectric coefficients d_{33} , d_{31} and d_{32} are expressed by equations (4)–(6). Since $\chi_3 \sqrt{2qN_d \chi_3 V_{bi}}$ is always positive, the signs of d_{33} , d_{31} and d_{32} are determined by the parts of these equations enclosed by brackets, that is, the transformed electrostriction coefficients. Here we set the ratio between the electrostriction coefficients as $Q_{12}^0/Q_{11}^0 = \nu$ and $Q_{44}^0/Q_{11}^0 = \eta$. Thus, the transformed electrostriction coefficients can be rewritten as follows:

$$Q'_{3333} = \frac{1}{16} Q_{11}^0 [(9 + 7\nu + 14\eta) + (1 - \nu - 2\eta)(4 \cos 2\theta + 3 \cos 4\theta)] \quad (11)$$

$$Q'_{1133} = \frac{1}{4} Q_{11}^0 [(1 + 3\nu - 2\eta) - (1 - \nu - 2\eta) \cos 2\theta] \quad (12)$$

$$Q'_{2233} = \frac{1}{16} Q_{11}^0 [(3 + 13\nu - 6\eta) - 3(1 - \nu - 2\eta) \cos 4\theta] \quad (13)$$

According to these equations, the possibility to have the auxetic piezoelectric effect is determined by the values of ν and η . The maximum and minimum values of Q'_{3333} by varying angle θ are Q_{11}^0 and $\frac{1}{16}(5.33 + 10.67\nu + 21.34\eta)Q_{11}^0$, respectively. For most solid materials, the ratio ν between Q_{12}^0 and Q_{11}^0 can be approximated as Poisson's ratio, which is usually in the range of -0.3 to -0.2 . Also, Q_{44}^0 is usually of the same sign as Q_{11}^0 , that is, $\eta > 0$. Thus, Q'_{3333} is always of the same sign as Q_{11}^0 ; namely, the bracketed part on the right side of equation (11) is always positive. Therefore, to have the type II auxetic piezoelectric effect, one needs to have

$$(1 + 3\nu - 2\eta) - (1 - \nu - 2\eta) \cos 2\theta > 0, \theta \in [0, \pi] \quad (14)$$

or

$$(3 + 13\nu - 6\eta) - 3(1 - \nu - 2\eta) \cos 4\theta > 0, \theta \in [0, \pi]. \quad (15)$$

To satisfy the above equations, one needs to, respectively, have the following:

$$\eta < \frac{1+\nu}{2} \quad (16)$$

or

$$\eta < \frac{3+5\nu}{6}. \quad (17)$$

Since ν is negative, $(1+\nu)/2$ is larger than $(3+5\nu)/6$. Thus, the least condition to show the type II auxetic piezoelectric effect with one of d_{31} and d_{32} being positive is $\eta < (1+\nu)/2$. An example of the orientation-dependent electrostriction coefficient with $\eta < (1+\nu)/2$ is shown in Supplementary Fig. 18. In this case, Q'_{1133} turns positive, as Q'_{3333} , when angle θ gets close to 90° , which gives rise to the type II auxetic piezoelectric effect. Once η decreases further, that is, $(1+2\nu)/2 < \eta < (3+5\nu)/6$, there will exist two angle regions that exhibit the type II auxetic piezoelectric effect, marked in grey in Supplementary Fig. 18c. The three-dimensional variation of the electrostriction coefficients corresponding to Supplementary Fig. 18 is given in Supplementary Fig. 19.

To have both d_{31} and d_{32} being the same sign as d_{33} , η at least needs to satisfy the following:

$$\begin{aligned} (1+3\nu-2\eta) - (1-\nu-2\eta)\cos 2\theta \\ = (3+13\nu-6\eta) - 3(1-\nu-2\eta)\cos 4\theta > 0 \end{aligned} \quad (18)$$

which results in

$$\cos 2\theta = -\frac{1}{3} \quad (19)$$

and

$$\eta < \frac{1+2\nu}{2}. \quad (20)$$

Supplementary Fig. 18d shows the variation of the electrostriction coefficients with respect to the angle θ when $\eta < \frac{1+2\nu}{2}$. The angle range to show the auxetic piezoelectric effect is marked by yellow, and the ranges to show the type II auxetic piezoelectric effect are marked by grey. Supplementary Fig. 19d is the corresponding three-dimensional version.

Overall, the manifestation of the auxetic piezoelectric effect in a Schottky junction made of semiconductors of cubic structure mainly depends on the relative value of Q'_{44} with respect to that of Q'_{11} . The smaller Q'_{44} , the easier to have an auxetic piezoelectric effect. To have d_{33} , d_{32} and d_{31} of the same sign, one needs to have $\eta < \frac{1+2\nu}{2}$. Regarding semiconductors with other crystallographic structures, the same method exploited above can be used to identify the possibility of having an auxetic piezoelectric effect. One can use first-principles theory to calculate the electrostriction tensor of the material of interest and then use the tensor transformation method used in our work to decipher the crystallographic orientation dependence.

Sample preparation

Nb:SrTiO₃ and Nb:TiO₂ single crystals with different orientations (SurfaceNet) were first cleaned by acetone, isopropyl and water in an ultrasonic bath. The (112)-oriented Nb:SrTiO₃ substrates were prepared by Hefei Kejing Materials Technology. Afterward, the crystal surface was cleaned by oxygen plasma for 60 s before sputtering gold electrodes (Cressington sputter coater 208HR, or ET-NanoSputter from Anhui Epitaxy Technology). The ohmic contacts were formed by evaporating

a Pt (40 nm)/Al (10 nm) bilayer on the crystal surface. The SrTiO₃/Ba_{0.6}Sr_{0.4}TiO₃/BaTiO₃ superlattices were grown by the pulsed laser deposition method at 650 °C with an oxygen pressure of 0.15 mbar (ET-NanoPLD from Anhui Epitaxy Technology).

Characterization methods of the auxetic piezoelectric effect

The piezoelectric coefficients were evaluated by a direct experimental approach, that is, by applying to the sample a homogeneous dynamic stress and measuring the short-circuit current as the main output. To measure d_{33} , the Schottky junctions were clamped between two sapphire substrates coated with gold electrodes. Special care was taken to keep the sapphire substrate surface flat and clean as well as perfectly aligned and parallel to each other, to avoid any spurious effects arising from inhomogeneous strain. Au/Al₂O₃ plates applied the stress directly to the Schottky junction and collected the generated current (Supplementary Fig. 3a).

The measurement set-up for the transverse coefficients was the same as that used in our previous work (Supplementary Fig. 3b). The piezoelectric measurement set-up measures simultaneously both the piezoelectric current and the applied force (stress) using a force sensor. The generated current is first read by a transimpedance amplifier (DLPCA-200, Femto) and then displayed by oscilloscope as a waveform or measured by a lock-in amplifier as a vector signal.

Demonstration of the converse auxetic piezoelectric effect

To detect the converse effect of the demonstrated auxetic piezoelectric effect, especially the transverse deformation under external bias induced by d_{31} , we developed a voltage-induced bending measurement using a cantilever device configuration, which is similar to that of the piezoelectric bimorph actuator (Fig. 4a,b). We used a blade saw and polishing technique to prepare samples, prepared on Nb:SrTiO₃ substrates into the cantilever geometry. The dimension of the (001)-oriented superlattice cantilever was about 3.5 mm × 1.2 mm × 0.15 mm, and that of the (111)-oriented one was about 4.0 mm × 1.6 mm × 0.12 mm.

Once a voltage parallel to the built-in polarization was applied to the piezo-active layer (that is, the superlattice or depletion layer of the Schottky junction) of the cantilever, the piezoelectric effect occurred and induced stress/strain. In the case of the (001)-oriented superlattice, this voltage induced an out-of-plane expansion and in-plane contraction, which generated an in-plane compressive stress to the top surface of the piezo-inactive substrate and bent the cantilever upward (Fig. 4a). By contrast, in the case of the (111)-oriented superlattice, due to the auxetic nature of its piezo-effect, the same applied voltage induced expansion in both the out-of-plane and in-plane directions, which exerted an in-plane tensile stress to the top layer of the cantilever and bent the cantilever downward (Fig. 4b). Thus, the (001)- and (111)-oriented cantilevers bent in opposite directions under the application of the same voltage, since the auxetic piezo-effect happened in the (111)-oriented samples. To demonstrate this scenario, we applied an a.c. voltage to both cantilevers and measured their vibration using an atomic force microscopy tip that contacted the end of the cantilevers. In our measurement set-up, a positive sign of the voltage represented its direction being parallel to the built-in polarization, that is, pointing from the bottom layer (that is, Nb:SrTiO₃ here) to the top electrode (that is, Pt); a positive sign of the bending displacement at the end of the cantilevers meant a bending downward.

In addition to the vibration waveform shown in Fig. 4, we also measured the dependence of a cantilever vibration of both orientations on the a.c. voltage amplitude and frequency (Supplementary Fig. 20). The bending amplitude of both orientations increased linearly with the amplitude of the a.c. voltage. The vibration phase with respect to the a.c. voltage of the (001)-oriented cantilever almost retained a constant value of about 170° , while that of the (111)-oriented cantilever showed a phase of about -9° . This conforms to a negative sign of d_{31} in the (001)-oriented superlattice but a positive sign of d_{31} in the (111)-oriented

superlattice, that is, the auxetic feature. Both cantilevers showed a resonant frequency at around 10 kHz. The most important feature in Supplementary Fig. 20c,d is the opposite change of the vibration phase between the two orientations. With increasing a.c. voltage frequency and passing through the resonance, the vibration of the (001) cantilever changed from out of phase to almost in phase, while that of the (111) cantilever evolved from in phase to out of phase, further conforming to the opposite signs of their transverse piezo-coefficients. Experimental data on the converse auxetic piezoelectric effect of Nb:SrTiO₃ Schottky junctions are given in Supplementary Fig. 21.

Overall, these sophisticated characterizations clearly demonstrate the manifestation of both direct and converse auxetic piezoelectric effects in a symmetry-engineered tricolour superlattice, confirming the general nature of the auxetic piezoelectric effect. The results offer a promising platform to optimize the performance and exploit the potential of this emerging phenomenon.

Data availability

The dataset that supports the findings of this study is available at the University of Warwick open access research repository (<http://wrap.warwick.ac.uk/180001>).

Acknowledgements

We thank M. Crosbie and M. Crouch for technical support. We also appreciate the valuable discussion with A. Sanchez and Z. D. Luo. We thank T. Tian for providing us with piezoelectric ceramics to calibrate our set-up. We acknowledge the technique support from Anhui Epitaxy Technology Co., Ltd. This work was partially carried out at the USTC Center for Micro and Nanoscale Research and Fabrication at the University of Science and Technology of China (USTC). T.-Y.Z. and S.L. acknowledge the support from Research Center for Industries of the Future (RCIF) at Westlake University. The computational resource

is provided by Westlake High-Performance Computing Center.

Regarding funding, M.-M.Y. acknowledges the University of Warwick and Hefei National Laboratory for financial support of this work. The work was partly supported by the Engineering and Physical Sciences Research Council (EPSRC, UK) through grant nos EP/P025803/1 (M.A.) and EP/T027207/1 (M.A.).

Author contributions

M.-M.Y. conceived the idea, designed the project, developed the phenomenological theory, set up the measurement system, prepared the devices and collected the experimental data. A.B.R. and P.M.G. provided the Mo/4H-SiC junctions. T.-Y.Z. and S.L. performed the DFT calculation. H.-M.S. and M.-M.Y. prepared the tricolour superlattices. M.-M.Y. and M.A. discussed the results. M.-M.Y. wrote the manuscript with input from all the authors.

Competing interests

The authors declare no competing interests.

Additional information

Supplementary information The online version contains supplementary material available at <https://doi.org/10.1038/s41563-023-01736-5>.

Correspondence and requests for materials should be addressed to Ming-Min Yang or Marin Alexe.

Peer review information *Nature Materials* thanks Daesu Lee, Anna Morozovska and the other, anonymous, reviewer(s) for their contribution to the peer review of this work.

Reprints and permissions information is available at www.nature.com/reprints.